RESEARCH PAPER



Clone granular soils with mixed particle morphological characteristics by integrating spherical harmonics with Gaussian mixture model, expectation-maximization, and Dirichlet process

Quan Sun¹ · Junxing Zheng¹

Received: 7 November 2019/Accepted: 2 April 2020/Published online: 18 April 2020 © Springer-Verlag GmbH Germany, part of Springer Nature 2020

Abstract

Computers have been taught to clone granular soil particles for discrete element method simulations to alleviate difficulties of using three-dimensional imaging techniques for scanning a large number of particles. In this process, computers analyze a few scanned particles to extract morphological characteristics of the target soil, which are used to clone as many particles as necessary. However, many natural granular soils contain a wide range of particle shapes mixing more than one type of morphological characteristics, causing difficulties in cloning. This research aims to address this challenge by integrating spherical harmonics with Gaussian mixture model, expectation—maximization, and Dirichlet process. Spherical harmonics coefficients are used to characterize morphological information of the granular soil. Gaussian mixture model is used to fit a function to the mixed morphological characteristics. The expectation—maximization and Dirichlet process are used to estimate the fitting parameters in Gaussian mixture model. Then, Gaussian mixture model is used to generate new spherical harmonics coefficients and then generate new particles. The effectiveness and accuracy of the proposed methodology are verified using a Griffin sand. Although this approach is developed for granular soils, the proposed technique can also be used to clone other particulate materials.

Keywords Discrete element method \cdot Gaussian mixture model \cdot Granular particle generation \cdot Particle shape characterization \cdot Spherical harmonics \cdot X-ray computed tomography

1 Introduction

Particle shape profoundly affects the engineering behavior of granular soils. For example, experimental studies have shown that sands consisting of angular and elongated particles exhibit larger values of index void ratios, internal friction, dilatancy, constant volume friction angle, compressibility, and small-strain modulus than sands with rounded and spherical particles [2, 3, 7, 9, 10, 16, 18–20, 25, 27, 35, 42, 44, 52, 60–62, 68]. Therefore, realistic particle geometries have been increasingly used in

analytical and numerical methodologies for explaining the observed macro-mechanical behavior of granular soils. For example, realistic particles were increasingly used in the discrete element method (DEM) to more precisely simulate the realistic mechanical behavior of granular soils [59, 63, 66].

The realistic particles can be scanned by various three-dimensional (3D) imaging techniques, such as X-ray computed tomography (X-ray CT) [11, 12, 45–48, 73], laser scanning technique [5, 17, 21], optical interferometer [1, 37], stereophotography [64, 65, 67], and structured light technique [49]. The optical interferometer, stereophotography, and structured light can only obtain half particle geometries exposing to the field of review of cameras. The laser scanner and X-ray CT were able to scan 3D full particle geometries. However, the laser scanner must scan particles one by one, so considerable labor efforts and time must be required to scan many particles. X-ray computed tomography (CT) was an ideal technique, which can scan

quansun@iastate.edu

[✓] Junxing Zheng junxing@iastate.eduQuan Sun

Department of Civil, Construction and Environmental Engineering, Iowa State University, Ames, IA 50011, USA

many particles at the same time to obtain their full 3D geometries. However, X-ray CT technique was limited by the high-cost devices and their maintenance, extensive image processing skills, demanding computational efforts for data processing, and small scanning field of view.

The typical sizes of soil specimens for X-ray CT scans were approximately 12 mm in diameter and 24 mm in height in the existing studies [11, 12, 24, 45–48, 73]. Therefore, scanning a sufficient amount of soil particles for simulating a triaxial test in DEM (diameter = 50 mm, height = 100 mm) required approximately 70 scans. This issue is recently addressed by Semnani and Borja [41]. They developed a stochastic framework based on multiplepoint statistics that used high-resolution training images to enhance low-resolution images obtained over a large field of review. They evaluated the proposed approach using X-ray CT images of organic-rich Woodford shale obtained at two different resolutions. Results showed that the proposed technique can generate realistic high-resolution images of the microstructure of shale over a large field of review.

Due to the limitations of imaging techniques for obtaining 3D realistic particles, many techniques were developed by researchers to generate realistic particles by computers. These techniques can be divided into two categories. The techniques in the first category aimed to generate random particle geometries. For example, Voronoi-based spheropolyhedra algorithm introduced by Galindo-Torres and Pedroso [14] and Galindo-Torres and Muñoz [13] and a Fourier-Voronoi-based algorithm introduced by Mollon and Zhao [29–31] have been developed to generate realistic particles. These randomly shaped particles may not be precisely representative of real granular soil particles.

The second type of techniques aimed to clone a granular soil: a few of 3D particles were scanned by 3D imaging techniques and analyzed to obtain shape characteristics, which are used to generate as many particles as necessary to clone the target soil. The spherical harmonics technique was typically used by researchers for cloning soils. A few of 3D scanned particles were analyzed to determine their spherical harmonics coefficients, which are considered as morphological properties, or "morphological gene," of this soil. Then, probability techniques were used to add "gene mutation," which enabled a computer to create random morphological variances in the generated particles to prodifferent particle shapes [15, 26, 43, 46, 56, 57, 70–72]. These studies demonstrated that the particle shape distributions of original and cloned soils remarkably agreed with each other.

The spherical harmonics techniques demonstrated excellent results for granular soils containing particles with similar shapes [15, 26, 43, 56, 57, 70–72]. These particles

were sharing with similar spherical harmonics coefficients or similar morphological genes. However, some natural soils contained a wide range of particle shapes, and these particles did not necessarily have similar morphological genes, such as Griffin sand.

We randomly picked 403 particles from a Griffin sand and filled these particles into a plastic cylinder. A highresolution X-ray CT was used to scan the soil specimen with a spatial resolution of 10 μm/voxel. The obtained 3D volumetric images were processed by image segmentation techniques to identify individual soil particles. The first step was to use image thresholding techniques [36] to segment air and particles, resulting in a binary image, in which the soil particles had a voxel value of ones (white color), and the air had a voxel value of zeros (black color). In this binary image, the soil particles were contacting with each other. Therefore, the second step was to use an improved watershed analysis technique [48] to segment contacting particles. The segmented volumetric image is shown in Fig. 1a. Six typical particles are shown in Fig. 1b-g. Griffin sand contains particles having angular and elongated shapes as shown in Fig. 1b-d and rounded and spherical shapes as shown in Fig. 1e-g.

Seven particle shape descriptors were used in this study to quantify the particle shapes as shown in Table 1. These particle shape descriptors can be determined using 3D computational geometry techniques [34, 48, 58, 69]. Distributions of particle shape parameters are shown in Fig. 2. It is evident that Griffin sand included two types of particle shapes displaying a gap in shape distributions. We used spherical harmonics-based particle generation technique developed by Wei et al. [56] to generate 25,000 particles. The 3D computational geometry techniques were used to analyze particle shape distributions of generated particles, and results are also shown in Fig. 2.

The shape distributions of cloned and original Griffin sand do not match well due to the gap existing in shape distributions. Existing spherical harmonics techniques assumed that all the particles in the soil have similar morphological characteristics and determine one morphological gene for the soil. Therefore, these methods failed to clone the sands with mixed particle morphological characteristics. This study aimed to address this issue by integrating spherical harmonics with Gaussian mixture model, expectation-maximization, and Dirichlet process techniques. The proposed technique can evaluate how many types of particle morphological genes in the soil and extract each morphological gene. These different morphological genes were used to generate different types of particle shapes. This technique was effective and robust for cloning granular soils with complex and mixed particle morphological characteristics.



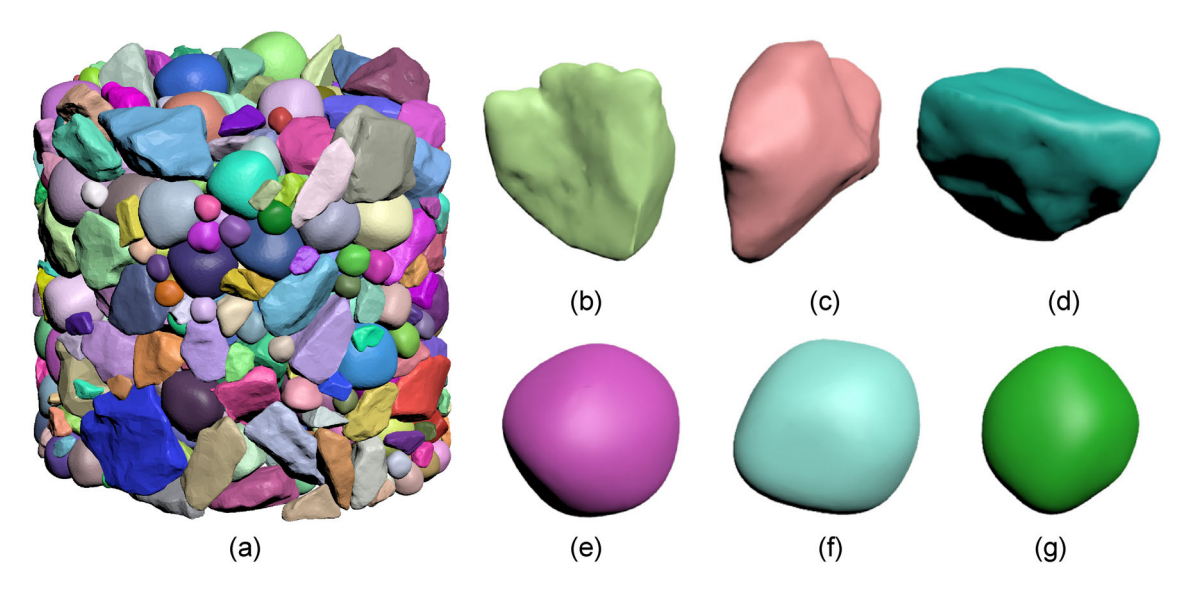


Fig. 1 3D Griffin sand specimen scanned by X-ray CT and six typical particles

Table 1 Commonly used shape descriptors and their definitions

Definitions (reference)		Formula	Note		
Convexity (solidity) [32]	3D	$C_x = \frac{V}{V_c}$	The ratio of the volume of the particle (V) to the volume of the minimum convex hull circumscribing the particle (V_c)		
Circularity [6]	3D	$C = \frac{6V}{\sqrt{\frac{A_s^3}{\pi}}}$	The ratio of the volume of the particle (V) to the volume of the sphere having the same surface area (A_s) as the particle		
Intercept sphericity [22]	3D	$S_{ m I}=\sqrt[3]{rac{d_2d_3}{d_1^2}}$	The cubic root of ratio of the product of the width of the particle (d_2) and the thickness of the particle (d_3) to the square of the length of the particle (d_1)		
Volume sphericity [40]	3D	$S_{ m V}=rac{V}{V_{ m cir}}$	The ratio of the volume of the particle (V) to the volume of the smallest circumscribed sphere $(V_{\rm cir})$		
Diameter sphericity [53]	3D	$S_{ m D}=rac{D_{e,3}}{D_{c,3}}$ $S_{ m A}=rac{A_e}{A_s}$	The ratio of the diameter of a sphere having the same volume as the original particle $(D_{\rm e,3})$ to the diameter of the minimum circumscribed sphere $(D_{\rm c,3})$		
Surface area sphericity [23]			The ratio of the surface area of the sphere having the same volume as the particle (A_e) to the real surface area of the particle (A_s)		
Roundness [53–55]	3D	$R = \frac{\sum_{i=1}^{N} r_{3,i} / N}{r_{\text{ins,3}}}$	The ratio of the average radius of spheres fitting the corners of the 3D particle geometry (r_3) to the radius of the maximum inscribed sphere to the 3D particle geometry $(r_{ins,3})$		

2 Spherical harmonics for particle generation

A 3D particle surface can be represented by the spherical harmonics coefficients c_n^m and spherical harmonics functions $Y_n^m(\theta, \varphi)$ [33]:

$$r(\theta, \varphi) = \sum_{n=-n}^{\infty} \sum_{m=-n}^{n} c_n^m Y_n^m(\theta, \varphi)$$
 (1)

where $r(\theta, \varphi)$ $(\theta \in [0, \pi], \varphi \in [0, 2\pi])$ is coordinates of

points on particle surface in the spherical coordinate system. The n and m are the degree and order of spherical harmonics, respectively. The base functions $Y_n^m(\theta, \varphi)$ can be determined as [57]:

$$Y_n^m(\theta,\varphi) = \sqrt{\frac{(2n+1)(n-m)!}{4\pi(n+m)!}} P_n^m \cos(\theta) e^{im\varphi}$$
 (2)

where P_n^m is Legendre function. The Legendre function can be expanded by Rodrigures's formula [56]:



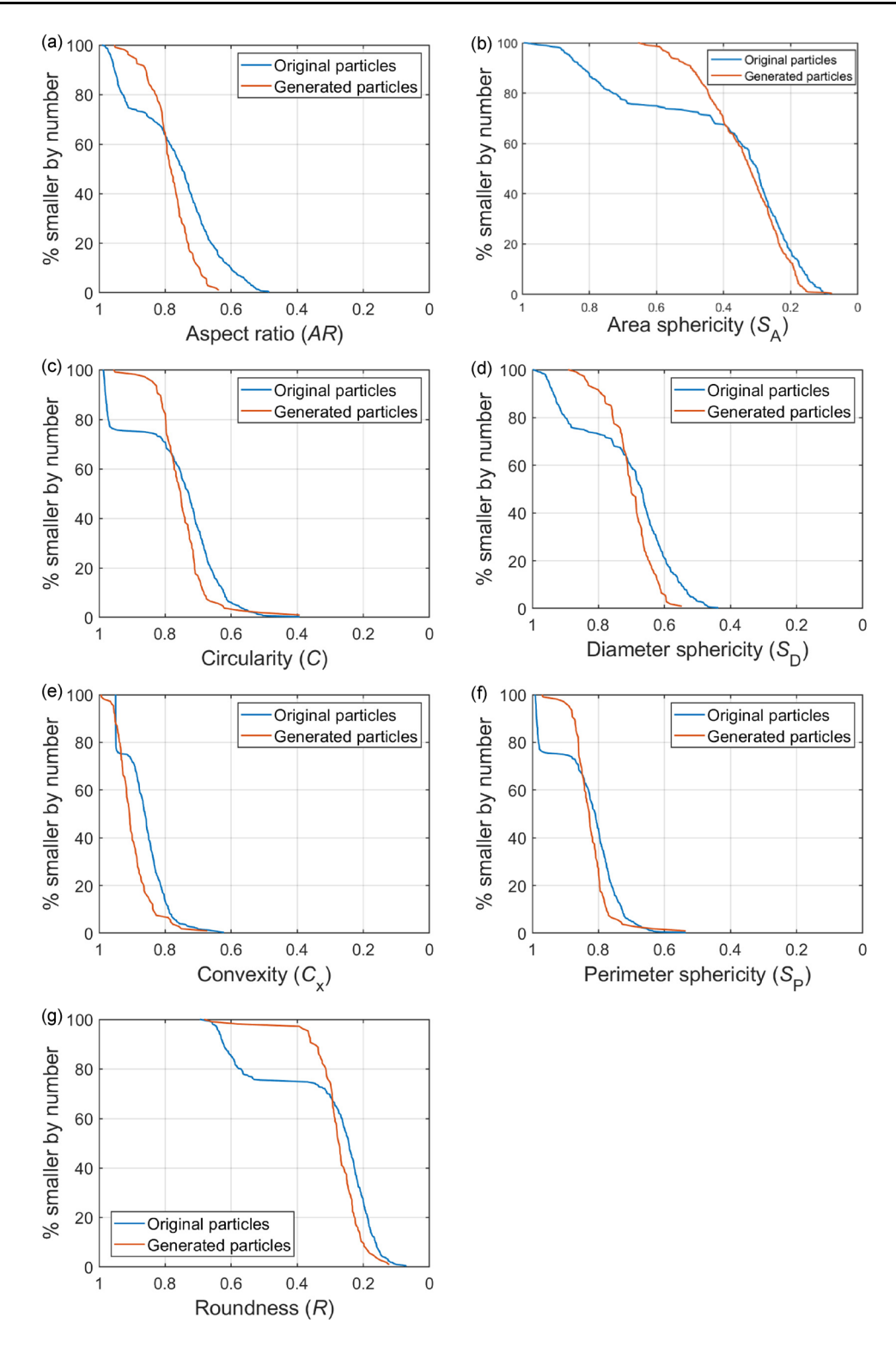


Fig. 2 Distributions of particle shape descriptors for original and cloned griffin sands by spherical harmonics algorithm

$$P_n^m(x) = (1 - x^2)^{|m|/2} \cdot \frac{\mathrm{d}^{|m|}}{\mathrm{d}x^{|m|}} \left[\frac{1}{2^n n!} \cdot \frac{\mathrm{d}^n}{\mathrm{d}x^n} (x^2 - 1)^n \right]. \tag{3}$$

Figures 3a, b illustrate the $Y_n^m(\theta, \varphi)$ and c_n^m for n = 0, 1, and 2. The spherical harmonics coefficients c_n^m are unique for a particle. As shown in Fig. 3b, the zero degree (n = 0)



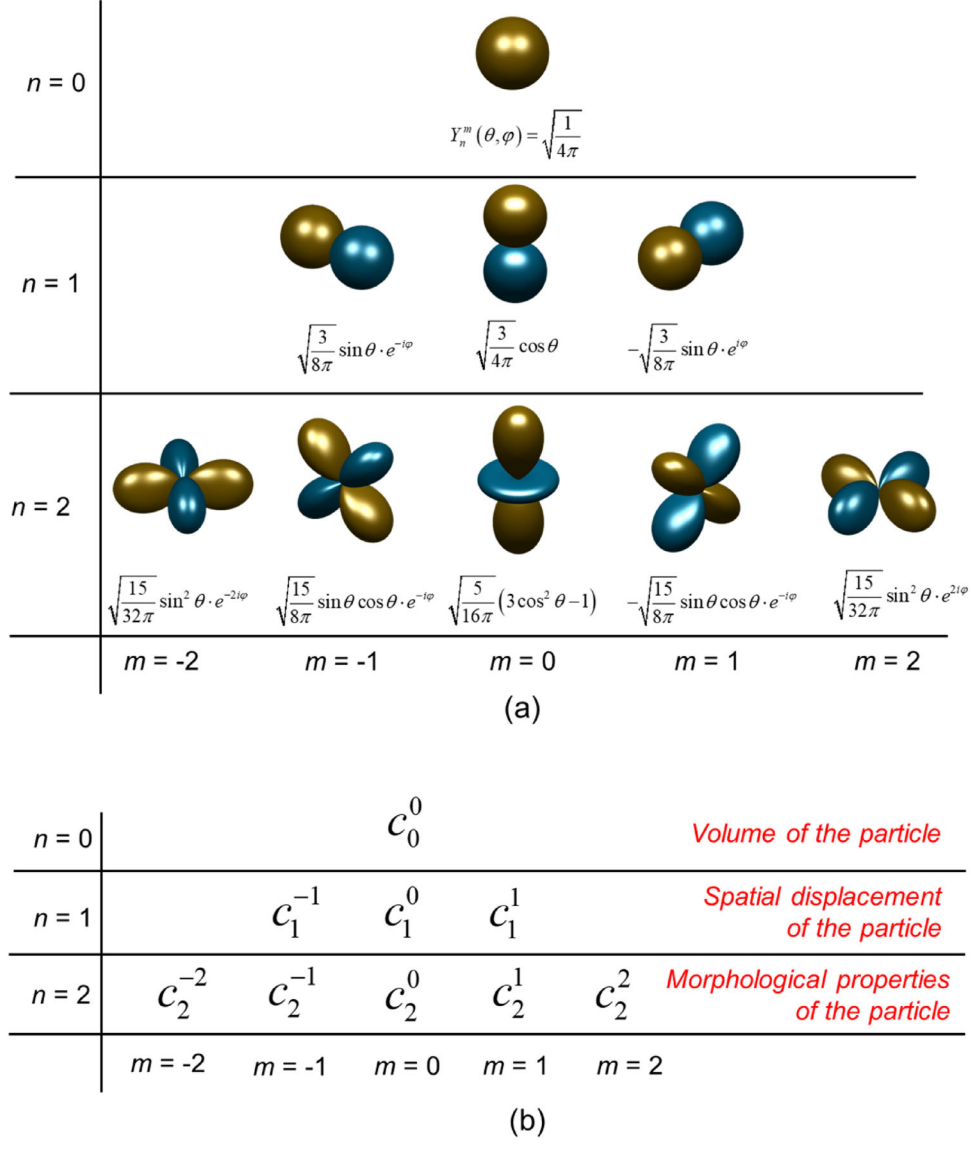


Fig. 3 Expansion of spherical harmonics for the first two degrees

of spherical harmonics coefficient c_0^0 determines the volume of the particle; the first degree of spherical harmonics coefficients (n=1), including c_1^1 , c_1^{-1} , and c_1^0 , determine the spatial displacement of the particle relative to origin; and the second degree of spherical harmonics coefficients (n=2), including c_2^{-2} , c_2^2 , c_2^0 , c_2^{-1} , and c_2^1 , store morphological properties of the particle. Despite not displaying in Fig. 3b, the larger degrees of spherical harmonics coefficients (n>2) also store morphological properties of the particle. Naturally, more detailed morphological properties of the particle will be contained for higher degrees n in spherical harmonics, so generated particles will be closer to the original particles if containing higher degrees of spherical harmonics coefficients. However, high degrees

will significantly increase computational loads. Researchers [31, 56, 57] have found that n = 15 provides satisfactory accuracy for particle representation and generation. Therefore, n = 15 was also used in this study.

The spherical harmonics coefficients c_n^m are a complex number:

$$c_n^m = a_n^m + b_n^m \cdot i \tag{4}$$

where a_n^m and b_n^m are the real part and imaginary part. The second norm of c_n^m determines the amplitude of spherical harmonics at different degrees L_n :

$$L_n = \sqrt{\sum_{m=-n}^n \left\| c_n^m \right\|^2} \quad (n = 0, 1, 2, ..., 15)$$
 (5)



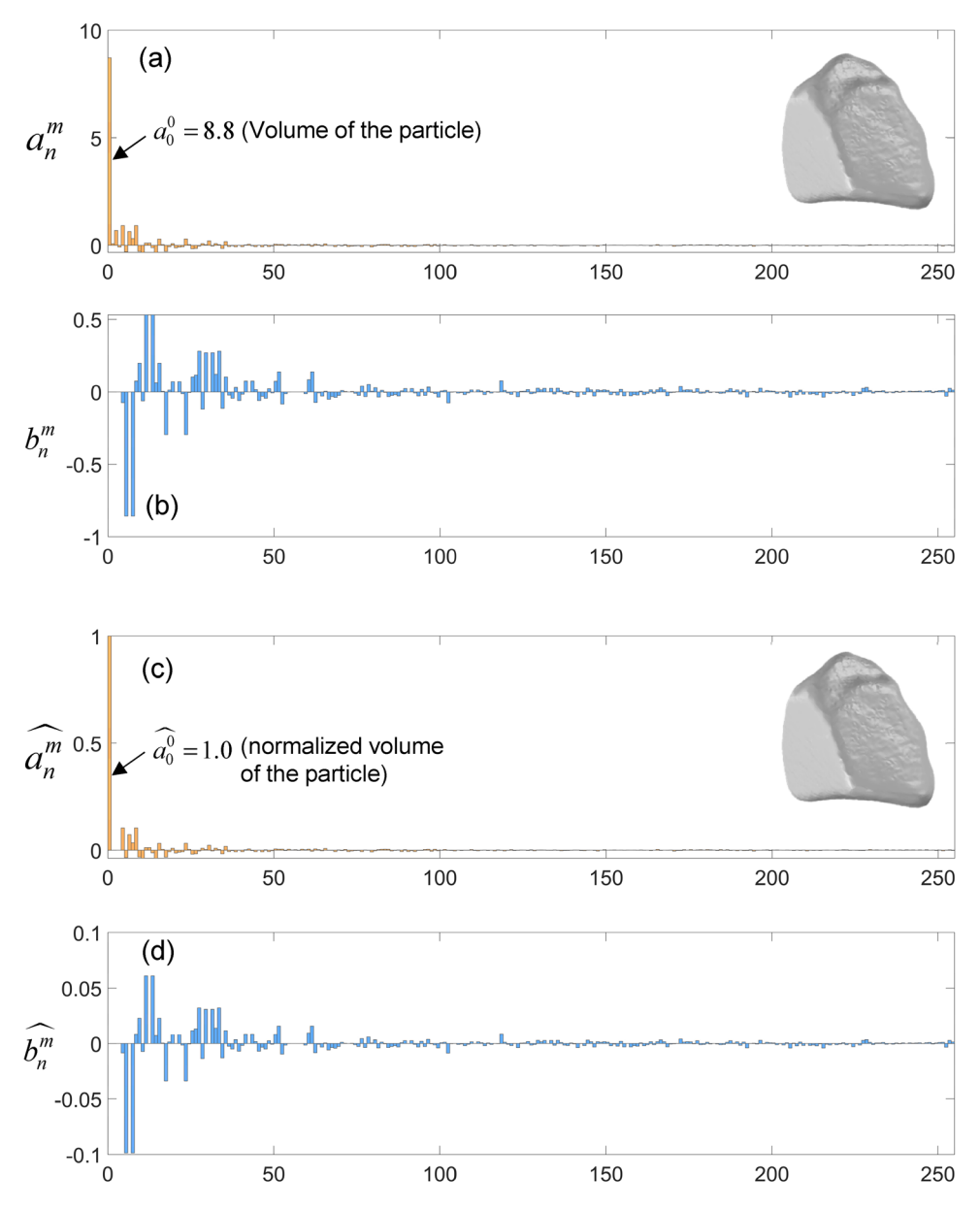


Fig. 4 The spherical harmonics coefficients and normalized spherical harmonics coefficients for a soil particle

The L_0 represents the volume of the particle. To remove the influence of particle volume, all the L_n can be divided by L_0 :

$$\frac{L_n}{L_0} = \sqrt{\sum_{m=-n}^{n} \left[\left(\frac{a_n^m}{L_0} \right)^2 + \left(\frac{b_n^m}{L_0} \right)^2 \right]} = \sqrt{\sum_{m=-n}^{n} \left\| \widehat{c_n^m} \right\|^2}$$
 (6)

Then, normalized spherical harmonics coefficients $\widehat{c_n^m}$ are defined by eliminating the effects of particle volume:

$$\widehat{c_n^m} = \widehat{a_n^m} + \widehat{b_n^m} \cdot i \tag{7}$$

where $\widehat{a_n^m}$ and $\widehat{b_n^m}$ are normalized real and imaginary parts correspondingly:

$$(6) \qquad \widehat{a_n^m} = \frac{a_n^m}{L_0} \tag{8}$$

$$\widehat{b_n^m} = \frac{b_n^m}{L_0} \tag{9}$$

A soil particle is shown in the insert of Fig. 4a. Spherical harmonics coefficients c_n^m of this particle were



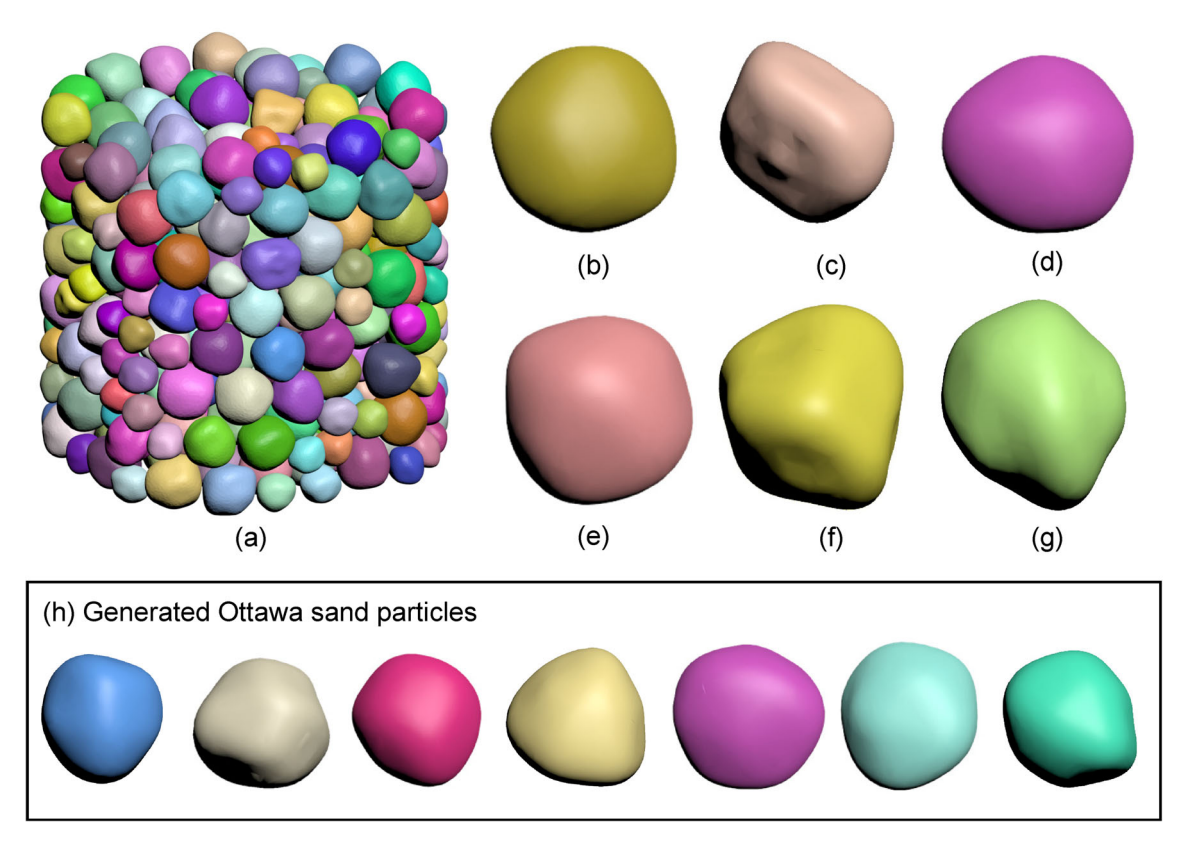


Fig. 5 3D Ottawa sand specimen scanned by X-ray CT and six typical particles

determined based on Eqs. (1)–(3). The degree n was set as 15. Therefore, a total of 256 spherical harmonics coefficients c_n^m were computed. These c_n^m values were complex numbers: the 256 real part a_n^m values are plotted in Fig. 4a, and the 256 imaginary part b_n^m values are plotted in Fig. 4b. The volume of the particle L_0 is computed as 8.8 based on Eq. (5), which was used to normalize spherical harmonics coefficients c_n^m to eliminate effects of volume. Therefore, the normalized real and imagery parts $\widehat{a_n^m}$ and $\widehat{b_n^m}$ were determined based on Eqs. (8) and (9), as shown in Fig. 4c, d.

The $\widehat{a_n^m}$ and $\widehat{b_n^m}$ stored the morphological properties of the particle, and they were independent of each other. Therefore, $\widehat{a_n^m}$ and $\widehat{b_n^m}$ together determined morphological genes of particles. If particles in a granular soil have similar shapes, their morphological genes should be also close to each other. For example, we scanned 450 Ottawa sand particles using X-ray CT as shown in Fig. 5a. Some typical particles are shown in Fig. 5b–g. The Ottawa sand particles all had well-rounded shapes, and their shapes were visually close to each other. Using Eqs. (1)–(9), $\widehat{a_n^m}$ and $\widehat{b_n^m}$ values of particles were computed. The histograms of $\widehat{a_n^m}$ and $\widehat{b_n^m}$ values for n = 2-15 are shown in Fig. 6a, b.

The $\widehat{a_n^m}$ and $\widehat{b_n^m}$ values of particles having similar morphological properties are close to each other and follow a Gaussian distribution. The same observation has been reported by Wei et al. [56].

The $\widehat{a_n^m}$ and $\widehat{b_n^m}$ values together determine the particle morphological gene. Therefore, a spherical harmonics descriptor was introduced by integrating $\widehat{a_n^m}$ and $\widehat{b_n^m}$ values by Wei et al. [56, 57] and Mollon and Zhao [31]:

$$D_n = \sqrt{\left(\widehat{a_n^m}\right)^2 + \left(\widehat{b_n^m}\right)^2} \tag{10}$$

The D_n distributions for n = 2-15 are shown in Fig. 6c, which also follow Gaussian distributions.

The distributions of $\widehat{a_n^m}$ and $\widehat{b_n^m}$ values or D_n values can be considered as the morphological gene of Ottawa sand. Gaussian functions were determined by fitting distributions of $\widehat{a_n^m}$ and $\widehat{b_n^m}$ values and plotted as solid lines as shown in Fig. 6. Then, these new $\widehat{a_n^m}$ and $\widehat{b_n^m}$ values can be generated based on the Gaussian functions. Then, the new $\widehat{a_n^m}$ and $\widehat{b_n^m}$ values can be input into Eq. (7) to generate a new set of normalized spherical harmonics coefficients $\widehat{c_n^m}$ values. Then the $\widehat{c_n^m}$ values can be used in Eqs. (1)–(3) to generate new particles. This was the basic concept of the exiting



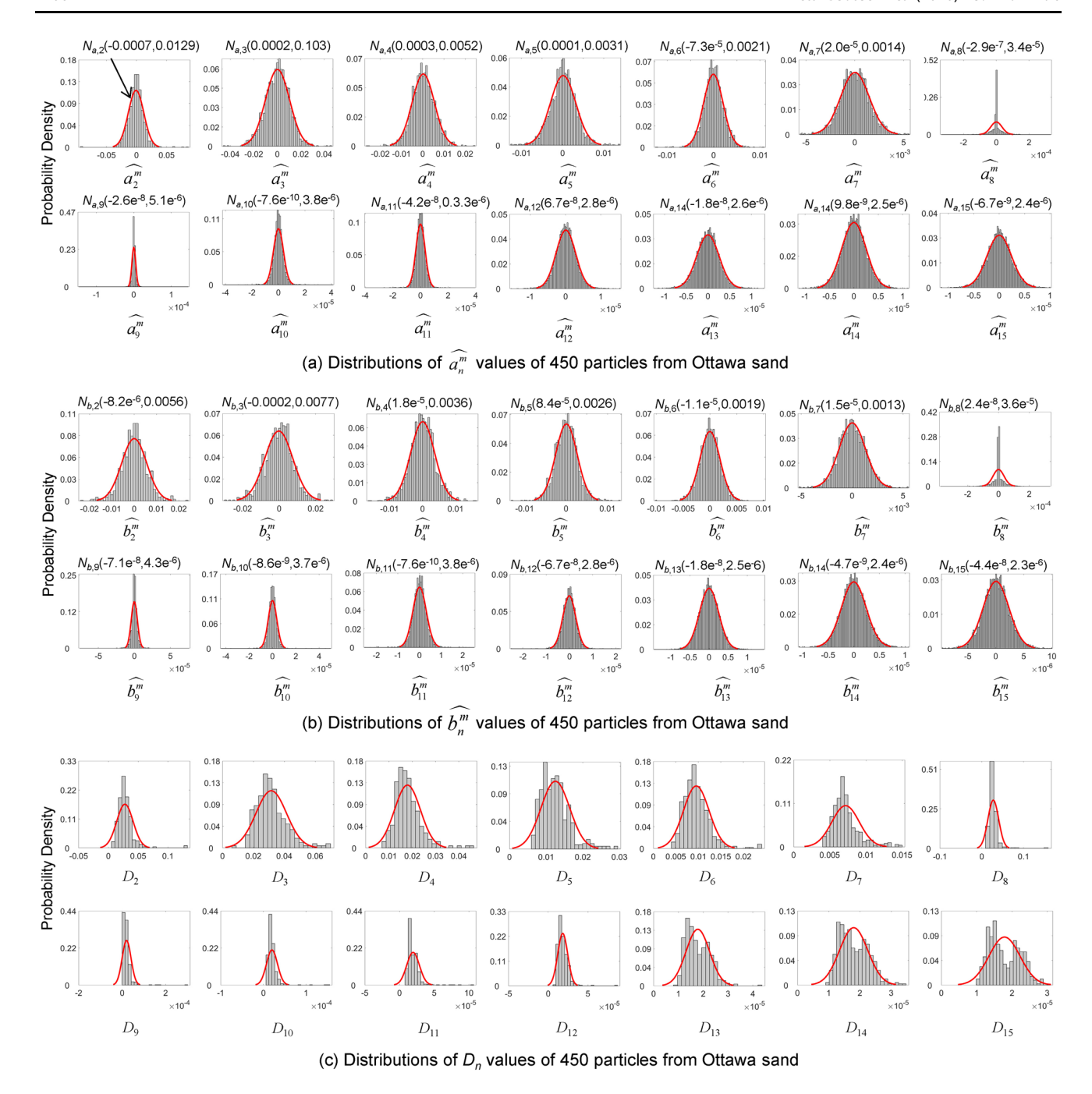


Fig. 6 The distributions of $\widehat{a_n^m}$, $\widehat{b_n^m}$, and D_n for n = 2-8 of 450 Ottawa sand particles

spherical harmonics techniques for cloning granular soils [15, 26, 43, 56, 57, 70–72].

It should be noted that newly generated particles had a unit volume because the normalized spherical harmonics coefficients $\widehat{c_n^m}$ values were used. Then, the generated particles can be up-scaled or down-scaled to match particle sizes, as will be shown later in the paper.

In Fig. 6a, b, the Gaussian functions were used to produce randomly $\widehat{a_n^m}$ and $\widehat{b_n^m}$ values and then these $\widehat{a_n^m}$ and $\widehat{b_n^m}$ values were used to generate 25,000 new Ottawa sand particles. The typically generated particles are shown in Fig. 5h, which visually have the same shape as original particles in Fig. 5a–g. Both original and cloned particles were analyzed by 3D computational geometry techniques [34, 48, 58] to determine particle shape descriptors. The



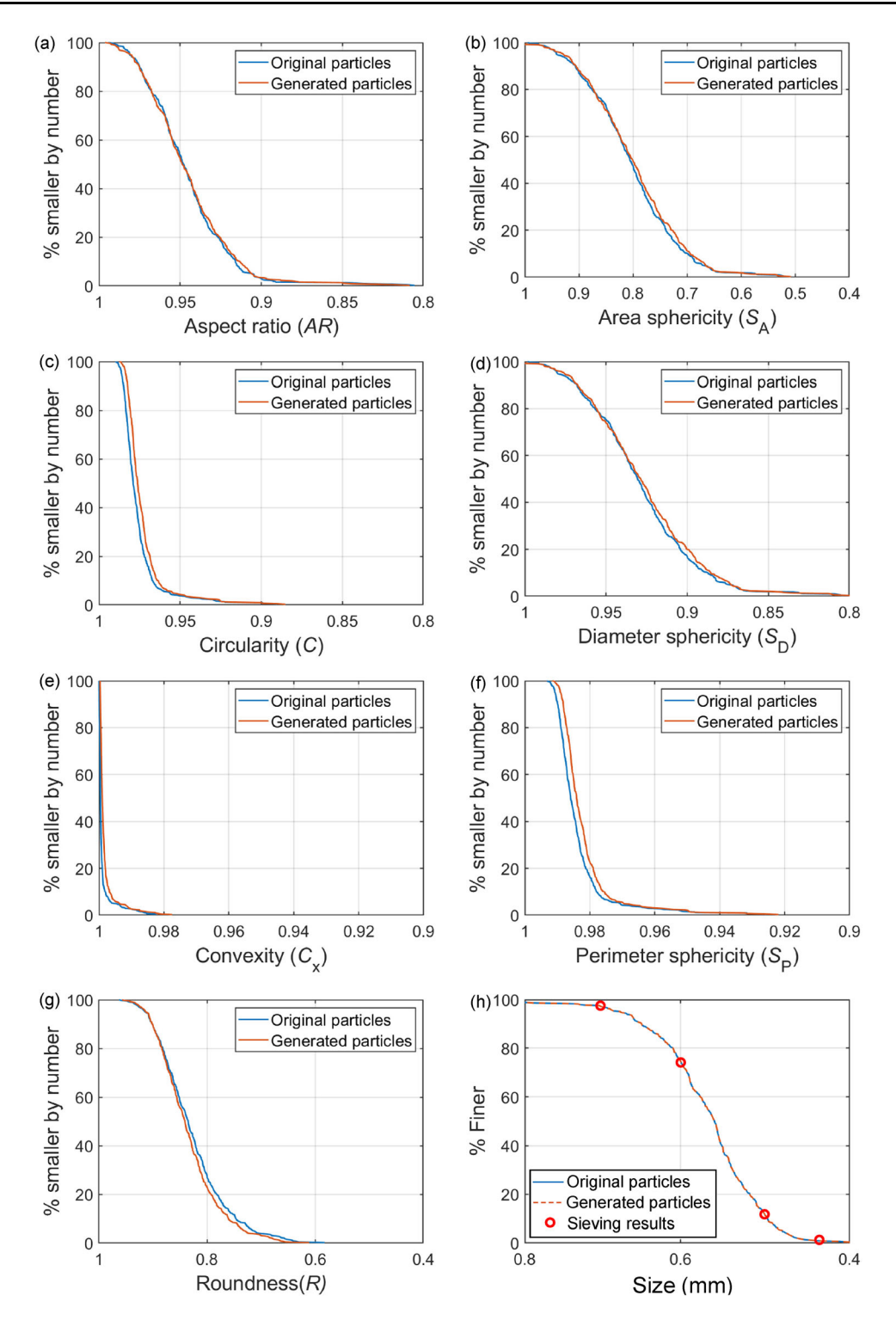


Fig. 7 Particle shape and size distributions of original and cloned Ottawa sands

particle shape distributions of original and cloned Ottawa sand remarkably agree with each other as shown in Fig. 7a-g.

The particle size distribution of the original 450 particles was analyzed by using both sieving test and 3D

computational geometry [48], and results agree with each other as shown in Fig. 7h. The 25,000 cloned particles all had a unit volume. Therefore, these particles were randomly up-scaled and down-scaled to match the particle distribution curve of original particles as shown in Fig. 7h.



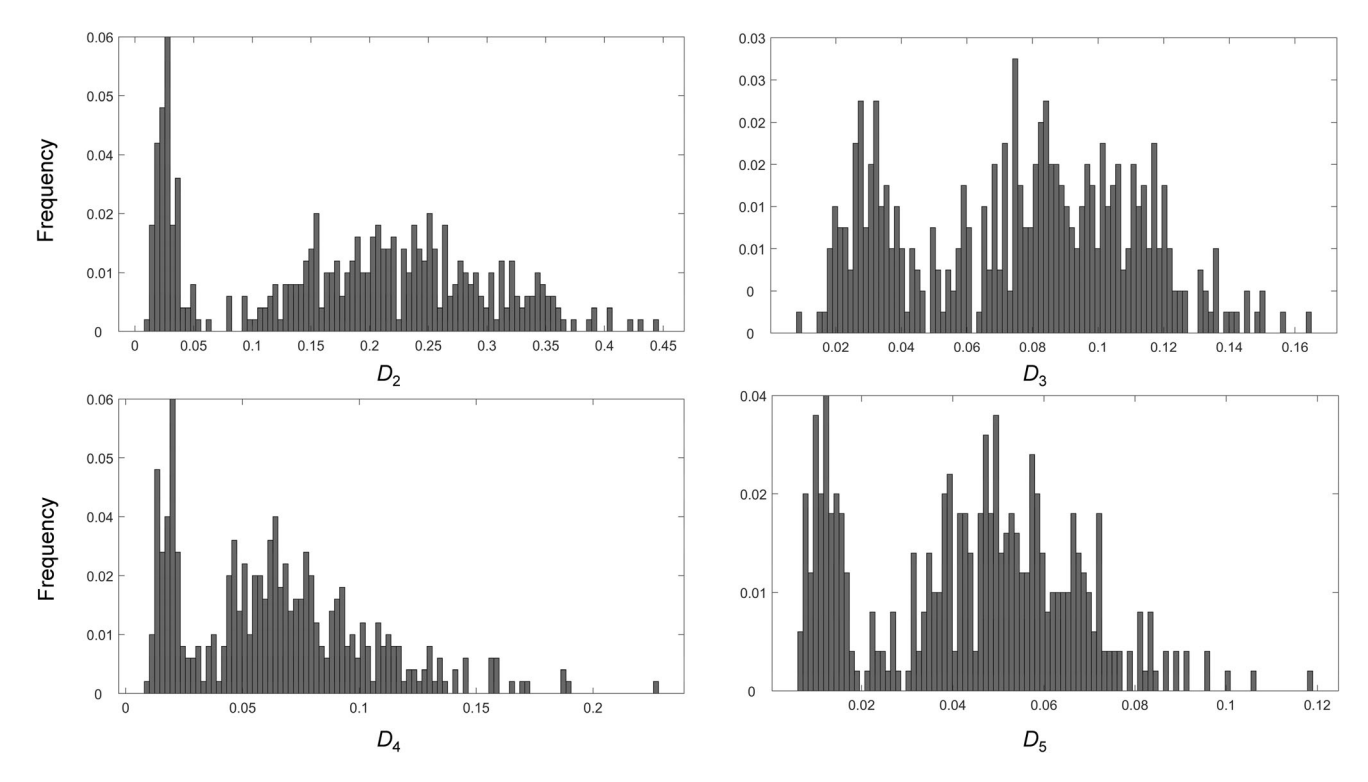


Fig. 8 Distributions of D_2 values of 403 particles of Griffin sand

Finally, the morphological gene of Ottawa sand (i.e., size and shape) has been successfully preserved in the cloned particles.

3 Gaussian Mixture Model (GMM) and Expectation–Maximization (EM) algorithm

The Griffin sand in Fig. 1 contains more than one type of particle morphological genes. The distribution of D_n values of the scanned 403 particles was determined, and histograms of D_2 , D_3 , D_4 , and D_5 values are shown in Fig. 9. (The distributions of other D_n values (n = 6, 7, ..., 15) are similar, so they are not plotted.)

Unlike Ottawa sand, the D_2 values of Griffin sand did not simply follow Gaussian distribution due to the mixed particle morphological characteristics. There were certainly other types of granular soils in nature with mixed particle morphological characteristics that possessed more complicated distributions of D_n values. Therefore, it was challenging to use a function to fit random distributions of D_n values. Therefore, a Gaussian mixture model (GMM) was introduced by this study to address this issue.

GMM is a probabilistic model using a finite number of Gaussian functions to fit complicated distributions of data

points. In other words, GMM divides data points into several groups and uses Gaussian function to fit data points in each group [4, 28]. The brief introduction of GMM is as follows.

Using the histogram of D_2 values in Fig. 8a as an example, the D_2 values can be divided into several groups and each group can be fitted by a Gaussian function. All these Gaussian functions together constitute the GMM. This progress essentially divided all the soil particles into several groups based on their morphological genes (D_2 values). Then, each group of particles with a similar morphological gene obeys their own Gaussian function, which is a component of GMM.

If a set of data points $X_1, X_2, X_3, ... X_i, ..., X_n$ follows a GMM consisting of k Gaussian functions, the GMM can be expressed as:

$$P(X_i|\theta) = \sum_{j=1}^k \alpha_j N(\mu_j, \Sigma_j)$$
(11)

where $N(\mu_j, \Sigma_j)$ is the *j*-th Gaussian function; μ is the expectation (or mean); \sum is covariance matrix; θ represents parameters for k Gaussian functions $\{\mu_1, \mu_2, \ldots, \mu_k, \sum_1, \sum_2, \ldots, \sum_k, \alpha_1, \alpha_2, \ldots, \alpha_k\}$; α_j $(j = 1, 2, \ldots, k)$ represents the weight of *j*-th Gaussian function in the GMM; and the summation of all α_j $(j = 1, 2, \ldots, \infty, \infty, \infty)$



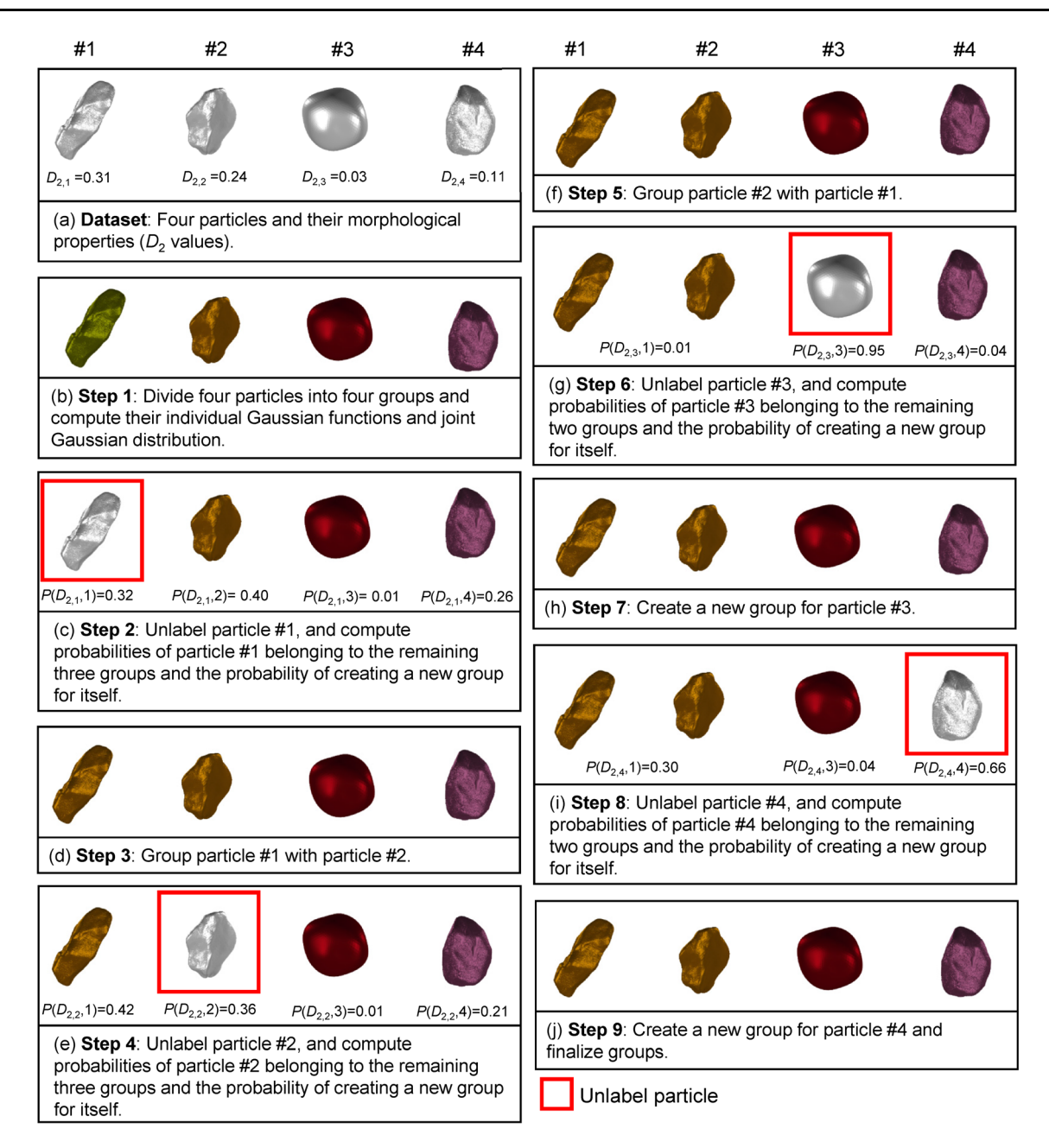


Fig. 9 The Dirichlet process algorithm for grouping soil particles

k) values is 1. The physical meaning of α_j is percentage of data points in the *j*-th group. For example, $\alpha_3 = 0.55$ means 55% percentage data points are in the group #3.

Expectation–Maximization (EM) algorithm was typically used to determine parameters in GMM $\theta = \{\mu_1, \mu_2, \dots, \mu_k, \sum_1, \sum_2, \dots, \sum_k, \alpha_1, \alpha_2, \dots, \alpha_k\}$ [8, 38]. For example, if the GMM contains three Gaussian functions (i.e., three groups), there will be a total of nine unknown parameters in GMM: $\mu_1, \mu_2, \mu_3, \Sigma_1, \Sigma_2, \Sigma_3, \alpha_1, \alpha_2,$ and α_3 . In the most application of EM, the number of groups is given by a priori. However, types of particle

morphological genes cannot be predicted for a soil, so the number of Gaussian functions in GMM cannot be determined by a priori. Therefore, we introduced Dirichlet process to solve this issue.

4 Dirichlet process (DP)

Dirichlet process (DP) is a stochastic process for dividing data into groups based on properties of data without specifying the number of groups a priori [50, 51].



(a) Oriç	ginal Griffin sand p	articles	(b) Generated Griffin sand particles		
Group 1 Angular particles	Group 2 Subangular particles	Group 3 Well-rounded particles	Group 1 Angular particles	Group 2 Subangular particles	Group 3 Well-rounded particles
			25.0		
Pa					
	To be the				

Fig. 10 The original and cloned particles of Griffin sand by the proposed technique in this study

Therefore, this study used DP to analyze the morphological properties of all the particles to determine how many types of particle morphological genes that soil has. In this research, D_2 values are used to represent the morphological property that DP is operating on.

Four randomly selected particles are used to conceptually illustrate the grouping process using DP in Fig. 9a. The goal is to group these particles based on their morphological genes (D_2 values). The D_2 values of #1, #2, #3 and #4 particles are computed as $D_{2,1} = 0.31$, $D_{2,2} = 0.24$, $D_{2,3} = 0.03$ and $D_{2,4} = 0.11$, respectively.

In the first step in Fig. 9b, four particles are divided into four groups (each particle forms a group). The D_2 value of each particle is used to fit a Gaussian function.

In the second step in Fig. 9c, we unlabel the #1 particle and evaluate the probability of this particle belonging to the remaining three groups, $P(D_{2,1},2)$, $P(D_{2,1},3)$ and

 $P(D_{2,1},4)$ and the probability of creating a new group for itself $P(D_{2,1},1)$. For example, the results are computed as $P(D_{2,1},2) = 0.40$, $P(D_{2,1},3) = 0.01$, $P(D_{2,1},4) = 0.26$ and $P(D_{2,1},1) = 0.32$. Clearly, $P(D_{2,1},2) = 0.40$ is the largest probability among these four values. Therefore, in the third step in Fig. 9d, particle #1 is grouped with #2 particles. Then the Gaussian function parameters of this group are updated due to the particle #1 being added.

In the fourth step in Fig. 9e, we unlabel the #2 particle and then calculate the probabilities of particle #2 belonging to the remaining three groups. For example, the results are computed as $P(D_{2,2},1) = 0.42$, $P(D_{2,2},3) = 0.01$, and $P(D_{2,2},4) = 0.21$ and the probability of creating a new group is computed as $P(D_{2,2},2) = 0.36$. Clearly, $P(D_{2,1},1) = 0.42$ is the largest probability among these four values. Then, in the fifth step in Fig. 9f, the particle #2 is grouped with the particle #1.



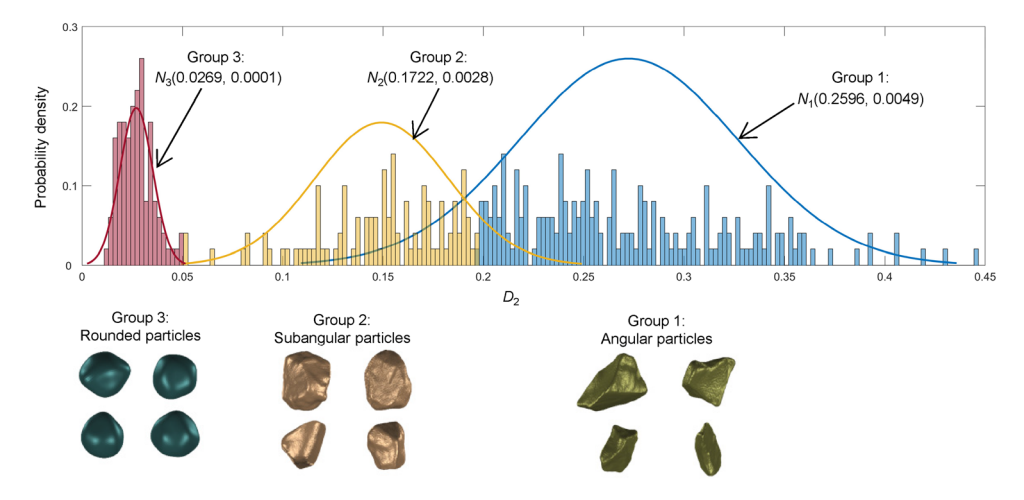


Fig. 11 Gaussian mixture model superimposed on D_2 distribution of Griffin sand

In the sixth step in Fig. 9g, we unlabel the #3 particle and then compute probabilities of particle #3 belonging to the remaining two groups, $P(D_{2,3},1) = 0.01$ and $P(D_{2,3},4) = 0.04$ and the probability of creating a new group, $P(D_{2,3},3) = 0.95$. Apparently, the probability of creating a new group is largest, so particle #3 creates a new group for itself, as shown in the seventh step in Fig. 9h.

We repeat this process for particle #4, which is classified into a new group, as shown in Fig. 9i, j. After labeling the four particles, the results are shown in Fig. 9j. Therefore, four sand particles are successfully divided into three groups based on their D_2 values (morphological characteristics). The same process can be conducted to group many particles.

5 Particle classification by Gaussian mixture model (GMM), expectation-maximization (EM), and Dirichlet process (DP)

The 403 Griffin sand particles in Fig. 1a were analyzed by spherical harmonics and their real and imagery parts $\widehat{a_n^m}$ and $\widehat{b_n^m}$ values and spherical harmonics descriptors D_n values were determined. Their D_2 values were input into Dirichlet process (DP) algorithm. The same process shown in Fig. 9 was repeated for 403 particles to classify the particles based on their morphological characteristics (D_2 values). This resulted in three groups. Therefore, three Gaussian functions were included in GMM.

Parameters for three Gaussian functions include $\theta = \{\mu_1, \mu_2, \mu_3, \sum_1, \sum_2, \sum_3, \alpha_1, \alpha_2, \alpha_3\}$. The GMM-EM optimization process was performed based on the D_2 values of these 403 particles. Then, the parameters for GMM were determined as

$$\theta = \begin{cases} \text{Group 1:} & \mu_1 = 0.2569 & \Sigma_1 = 0.0049 & \alpha_1 = 0.49 \\ \text{Group 2:} & \mu_2 = 0.1722 & \Sigma_2 = 0.0028 & \alpha_2 = 0.26 \\ \text{Group 3:} & \mu_3 = 0.0269 & \Sigma_3 = 0.0001 & \alpha_3 = 0.25 \end{cases}$$

$$(12)$$

The weights of three Gaussian functions in GMM are determined as $\alpha_1 = 0.49$, $\alpha_2 = 0.26$ $\alpha_3 = 0.25$, respectively. Some of particles in three groups are shown in Fig. 10a. The group 1 included 197 particles that had angular and elongated shapes. The group 2 included 105 particles that had subangular and elongated shapes. The group 3 included 101 particles that had rounded and spherical shapes.

The GMM is superimposed on the D_2 histogram in Fig. 11, which fits the distributions of D_2 values very well. The fractal dimension (FD) contains the information of spherical harmonics coefficients which is introduced. Quevedo et al. [39] proposed an empirical method to

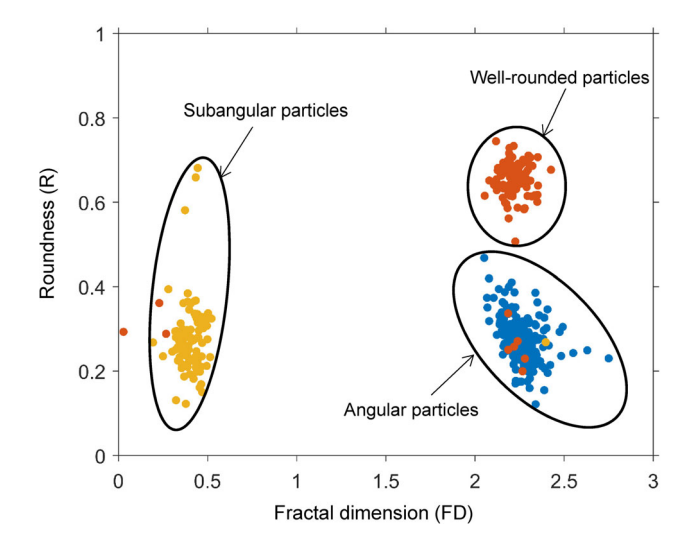


Fig. 12 The relationship between Fractal dimensions and roundnesses of particles of Griffin sand



determine the fractal dimension of spherical harmonics descriptor:

$$FD = 3 + \frac{\log(D_n)}{\log(n)} \tag{13}$$

where FD is the fractal dimension. The fractal dimension versus roundness is plotted in Fig. 12. The most data points

of one type of soil particles are concentrating, and three clusters were observed. This validates the effectiveness of accuracy of integrated GMM, EM, and DP algorithms for classifying particle morphological genes.

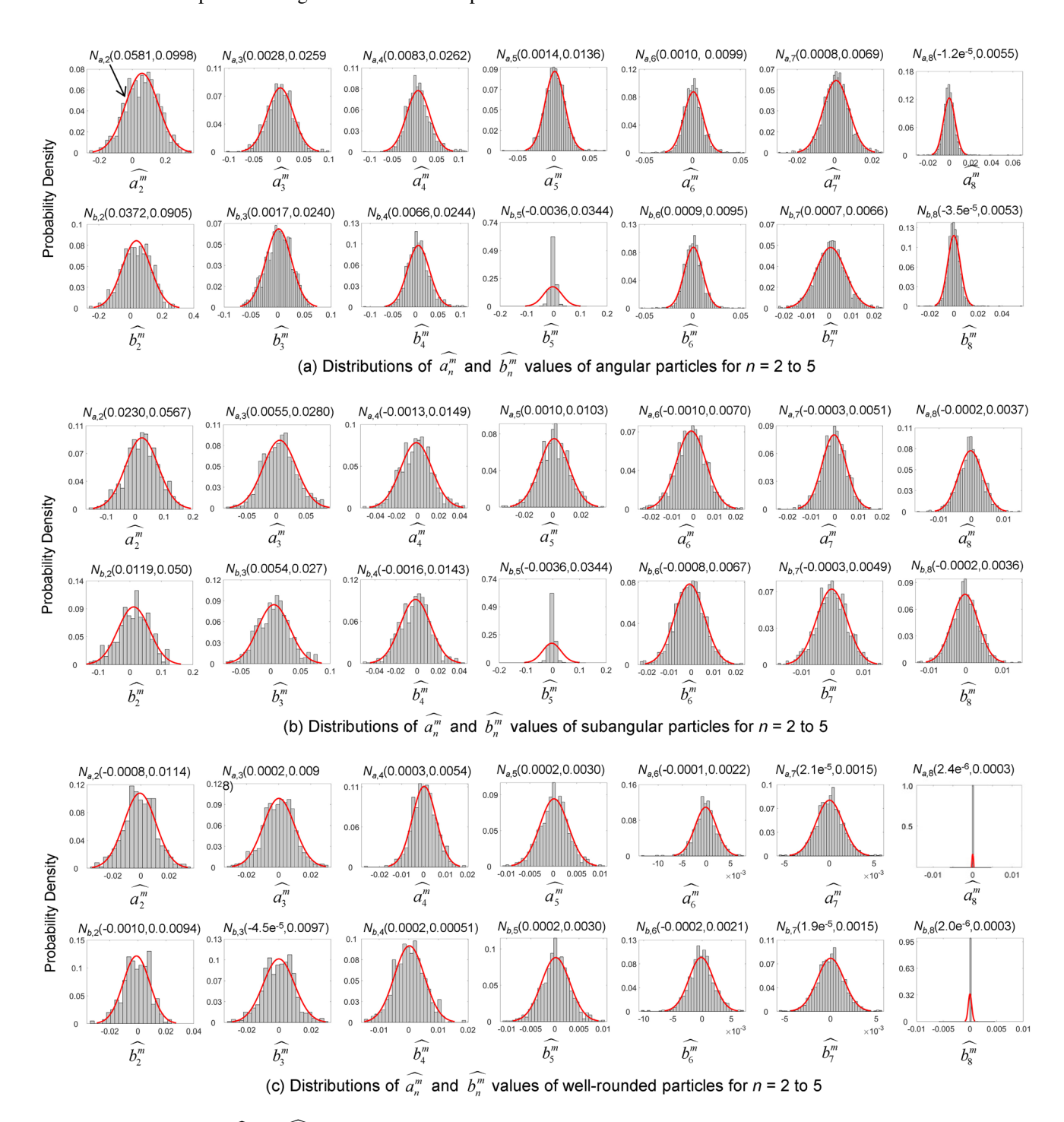


Fig. 13 The distribution of $\widehat{a_n^m}$ and $\widehat{b_n^m}$ for n = 2-8 of 403 Griffin sand particles



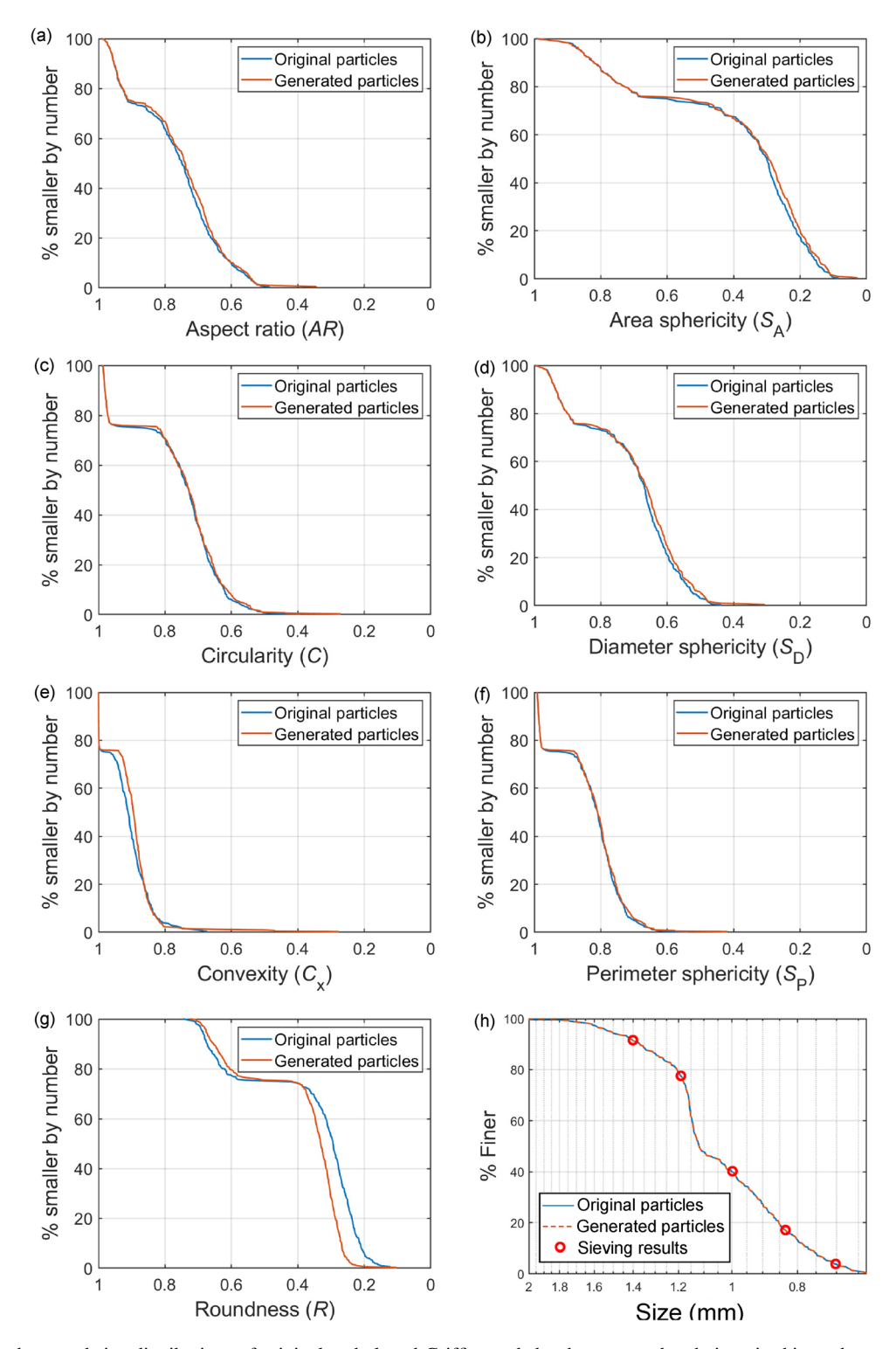


Fig. 14 Particle shape and size distributions of original and cloned Griffin sands by the proposed technique in this study

6 Cloning soil particles

The 403 Griffin sand particles have been classified into three groups. For each group of particles, their normalized harmonics coefficients $\widehat{a_n^m}$ and $\widehat{b_n^m}$ values can be plotted.

For example, Fig. 13 plots the $\widehat{a_n^m}$ and $\widehat{b_n^m}$ values for n=2-7 for each group of particles. The remaining $\widehat{a_n^m}$ and $\widehat{b_n^m}$ values for n=8-15 are similar, so they are not plotted in Fig. 13.



The Gaussian functions were fitted to $\widehat{a_n^m}$ and $\widehat{b_n^m}$ values of three types (i.e., very angular, subangular, and well rounded) of soil particles, respectively, as shown in Fig. 13. Then, new $\widehat{a_n^m}$ and $\widehat{b_n^m}$ values for three types of particles were generated based on the Gaussian distribution, and these new $\widehat{a_n^m}$ and $\widehat{b_n^m}$ values were used to generate new Griffin sand particles within three groups. For example, as shown in Fig. 13a, the distributions of $\widehat{a_2^m}$ and $\widehat{b_2^m}$ of angular particles are determined. Then, we drew new $\widehat{a_n^m}$ and $\widehat{b_n^m}$ (n = 2, 3, ..., 15) were also drawn from their own distribution randomly. Then the associated $\widehat{c_n^m}$ were obtained from Eq. (7). Applying Eqs. (1)–(3), a realistic angular particle was generated. Subangular and well-rounded particles could also be generated from their $\widehat{a_n^m}$ and $\widehat{b_n^m}$ distributions in Fig. 13b, c, respectively.

The weights of three Gaussian functions in GMM are determined as $\alpha_1 = 0.49$, $\alpha_2 = 0.26$ $\alpha_3 = 0.25$, respectively. Therefore, the percentage ratios of generated particles must obey 49:26:25 in very angular, subangular, and well-rounded groups, respectively. Therefore, we generated 12,250 very angular particles, 6500 subangular particles, and 6250 well-rounded particles. A total of 25,000 particles were generated.

Generated particles and original particle are compared in Fig. 10. They are visually very similar. The shape distributions of the original 403 particles and generated 25,000 particles are compared in Fig. 14a–g. Their shape distributions remarkably agree with each other. Therefore, the particle shapes of Griffin sand were successfully cloned by the proposed study.

Finally, the particle sizes of the original 403 particles were determined using computational geometry [48] and sieve analysis as shown in Fig. 14h. The optical and sieving results agree with each other, validating effectiveness of optical based particle size quantification. The generated 25,000 particles are randomly scaled up or scaled down to match the particle size distributions as shown in Fig. 14h. Therefore, the cloned Griffin sand particles successfully preserved both particle shape and size characteristics of original Griffin sand.

The proposed method was effective and accurate to clone granular soil with mixed particle morphological characteristics. Although the framework (spherical harmonics, GMM, EM, and DP) is developed based on granular soils, this framework can be used to clone other particulate materials with mixed particle shapes.

7 Conclusion

The natural soils, such as Griffin sand, contain particles with a mixture of morphological characteristics, or different morphological genes. This research integrates spherical harmonics, Gaussian mixture model, expectation-maximization, and Dirichlet process to clone such granular soils with mixed particle morphological genes. Spherical harmonics coefficients are used to extract morphological genes of the particles. Gaussian mixture model, expectation-maximization, and Dirichlet process analyze spherical harmonics coefficients to determine the types of morphological genes and their percentages. The Gaussian function is determined for each type of morphological gene, forming a Gaussian mixture model. The Gaussian mixture model is used to generate new spherical harmonics coefficients, which are used to generate new soil particles. The particle shape and size distributions of generated particles agree well with target soil. The proposed technique can also be used to clone other particulate materials with a mixture of particle shapes.

Acknowledgements This material is based upon work supported by the US National Science Foundation under Grant No. CMMI 1917332. Any opinions, findings, and conclusions or recommendations expressed in this material are those of the authors and do not necessarily reflect the views of the National Science Foundation.

Compliance with ethical standards

Conflict of interest The authors declare that they have no conflict of interest.

References

- 1. Alshibli KA, Alsaleh MI (2004) Characterizing surface roughness and shape of sands using digital microscopy. J Comput Civ Eng 18:36–45. https://doi.org/10.1061/~ASCE!0887-3801~2004!18:1~36!
- Alshibli KA, Cil MB (2018) Influence of particle morphology on the friction and dilatancy of sand. J Geotech Geoenviron Eng 144:04017118. https://doi.org/10.1061/(ASCE)GT.1943-5606. 0001841
- Altuhafi FN, Coop MR, Georgiannou VN (2016) Effect of particle shape on the mechanical properties of natural sands.
 J Geotech Geoenviron Eng 142:1–15. https://doi.org/10.1061/ (ASCE)GT.1943-5606.0001569
- Amendola C, Faugere JC, Sturmfels B (2016) Moment varieties of gaussian mixtures. J Algebr Stat 7:14–28. https://doi.org/10. 18409/jas.v7i1.42
- Anochie-Boateng JK, Komba JJ, Mvelase GM (2013) Three-dimensional laser scanning technique to quantify aggregate and ballast shape properties. Constr Build Mater 43:389–398. https:// doi.org/10.1016/j.conbuildmat.2013.02.062
- Aschenbrenner BC (1956) A new method of expressing particle sphericity. J Sediment Res 26:15–31. https://doi.org/10.1306/ 74D704A7-2B21-11D7-8648000102C1865D



- Bareither CA, Edil TB, Benson CH, Mickelson DM (2008) Geological and physical factors affecting the friction angle of compacted sands. J Geotech Geoenviron Eng 134:1476–1489. https://doi.org/10.1061/(asce)1090-0241(2008)134:10(1476)
- Biernacki C, Celeux G, Govaert G (2003) Choosing starting values for the EM algorithm for getting the highest likehood in multivariate Gaussian mixture models. Comput Stat Data Anal 41:561–575. https://doi.org/10.1016/S0167-9473(02)00163-9
- Cavarretta I, O'Sullivan C, Coop MR (2010) The influence of particle characteristics on the behaviour of coarse grained soils. Geotechnique 60:413–423. https://doi.org/10.1680/geot.2010.60. 6.413
- Cho G-C, Dodds J, Santamarina JC (2006) Particle shape effects on packing density, stiffness, and strength: natural and crushed sands. J Geotech Geoenviron Eng 132:591–602. https://doi.org/ 10.1061/(asce)1090-0241(2006)132:5(591)
- Cil MB, Alshibli KA, Kenesei P (2017) 3D experimental measurement of lattice strain and fracture behavior of sand particles using synchrotron X-ray diffraction and tomography. J Geotech Geoenvirom Eng 143:1–18. https://doi.org/10.1061/(ASCE)GT. 1943-5606.0001737
- Druckrey AM, Alshibli KA, Al-Raoush RI (2016) 3D characterization of sand particle-to-particle contact and morphology. Comput Geotech 74:26–35. https://doi.org/10.1016/j.compgeo. 2015.12.014
- Galindo-Torres SA, Muñoz JD, Alonso-Marroquín F (2010) Minkowski-Voronoi diagrams as a method to generate random packings of spheropolygons for the simulation of soils. Phys Rev E Stat Nonlinear Soft Matter Phys 82:1–12. https://doi.org/10. 1103/PhysRevE.82.056713
- Galindo-Torres SA, Pedroso DM, Muñoz JD, Alonso-Marroquín F (2010) Molecular dynamics simulations of complex-shaped particles using Voronoi-based spheropolyhedra. Phys Rev E. https://doi.org/10.1103/physreve.81.061303
- Grigoriu M, Garboczi E, Kafali C (2006) Spherical harmonic-based random fields for aggregates used in concrete. Powder Technol 166:123–138. https://doi.org/10.1016/j.powtec.2006.03. 026
- Guida G, Viggiani GMB, Casini F (2009) Multi-scale morphological descriptors from the fractal analysis of particle contour. Acta Geotech. https://doi.org/10.1007/s11440-019-00772-3
- Hayakawa Y, Oguchi T (2005) Evaluation of gravel sphericity and roundness based on surface-area measurement with a laser scanner. Comput Geosci 31:735–741. https://doi.org/10.1016/j. cageo.2005.01.004
- Hryciw RD, Zheng J, Shetler K (2016) Particle roundness and sphericity from images of assemblies by chart estimates and computer methods. J Geotech Geoenviron Eng. https://doi.org/10. 1061/(ASCE)GT.1943-5606.0001485
- Jerves AX, Kawamoto RY, Andrade JE (2016) Effects of grain morphology on critical state: a computational analysis. Acta Geotech 11:493–503. https://doi.org/10.1007/s11440-015-0422-8
- Kandasami R, Murthy T (2014) Effect of particle shape on the mechanical response of a granular ensemble. 3rd International symposium on geomechanics from micro to macro. Univ Cambridge, Cambridge, pp 1093–1098
- Kim H, Haas CT, Rauch AF, Browne C (2002) Dimensional ratios for stone aggregates from three-dimensional laser scans.
 J Comput Civ Eng 16:175–183. https://doi.org/10.1061/ (ASCE)0887-3801(2002)16:3(175)
- Krumbein WC, Sloss LL (1951) Stratigraphy and sedimentation.
 W.H Freeman and Company, San Francisco
- Kuo C-Y, Freeman R (2000) Imaging indices for quantification of shape, angularity, and surface texture of aggregates. Transp Res Rec J Transp Res Board 1721:57–65. https://doi.org/10.3141/ 1721-07

- Lai Z, Chen Q (2019) Reconstructing granular particles from X-ray computed tomography using the TWS machine learning tool and the level set method. Acta Geotech 14:1–18. https://doi. org/10.1007/s11440-018-0759-x
- Li C, Zheng J, Zhang Z et al (2020) Morphology-based indices and recommended sampling sizes for using image-based methods to quantify degradations of compacted aggregate materials. Constr Build Mater 230:116970. https://doi.org/10.1016/j.con buildmat.2019.116970
- Liu X, Garboczi EJ, Grigoriu M et al (2011) Spherical harmonic-based random fields based on real particle 3D data: improved numerical algorithm and quantitative comparison to real particles. Powder Technol 207:78–86. https://doi.org/10.1016/j.powtec. 2010.10.012
- Liu X, Yang J (2018) Shear wave velocity in sand: effect of grain shape. Géotechnique 68:742–748. https://doi.org/10.1680/jgeot. 17 t 011
- Melnykov V, Melnykov I (2012) Initializing the em algorithm in Gaussian mixture models with an unknown number of components. Comput Stat Data Anal 56:1381–1395. https://doi.org/10. 1016/j.csda.2011.11.002
- Mollon G, Zhao J (2012) Fourier–Voronoi-based generation of realistic samples for discrete modelling of granular materials. Granul Matter 14:621–638. https://doi.org/10.1007/s10035-012-0356-x
- Mollon G, Zhao J (2013) Generating realistic 3D sand particles using Fourier descriptors. Granul Matter 15:95–108. https://doi. org/10.1007/s10035-012-0380-x
- Mollon G, Zhao J (2014) 3D generation of realistic granular samples based on random fields theory and Fourier shape descriptors. Comput Methods Appl Mech Eng 279:46–65. https:// doi.org/10.1016/j.cma.2014.06.022
- Mora CF, Kwan AKH (2000) Sphericity, shape factor, and convexity measurement of coarse aggregate for concrete using digital image processing. Cem Concr Res 30:351–358. https://doi.org/10.1016/S0008-8846(99)00259-8
- 33. Müller C (2006) Spherical harmonics. Springer, Berlin
- 34. Nie Z, Liang Z, Wang X (2018) A three-dimensional particle roundness evaluation method. Granul Matter 20:1–11. https://doi.org/10.1007/s10035-018-0802-5
- Nouguier-Lehon C, Cambou B, Vincens E (2003) Influence of particle shape and angularity on the behaviour of granular materials: a numerical analysis. Int J Numer Anal Methods Geomech 27:1207–1226. https://doi.org/10.1002/nag.314
- 36. Otsu N (1979) A threshold selection method from gray-level histograms. IEEE Trans Syst Man Cybern 9:62–66
- Otsubo M, O'Sullivan C, Sim WW, Ibraim E (2015) Quantitative assessment of the influence of surface roughness on soil stiffness. Géotechnique 65:694–700. https://doi.org/10.1680/geot.14.T.028
- Pernkopf F, Bouchaffra D (2005) Genetic-based EM algorithm for learning Gaussian mixture models. IEEE Trans Pattern Anal Mach Intell 27:1344–1348. https://doi.org/10.1109/TPAMI.2005. 162
- Quevedo R, Carlos LG, Aguilera JM, Cadoche L (2002) Description of food surfaces and microstructural changes using fractal image texture analysis. J Food Eng 53:361–371. https:// doi.org/10.1016/S0260-8774(01)00177-7
- Riley NA (1941) Projection sphericity. SEPM J Sediment Res. https://doi.org/10.1306/d426910c-2b26-11d7-8648000102c1865d
- Semnani SJ, Borja RI (2017) Quantifying the heterogeneity of shale through statistical combination of imaging across scales. Acta Geotech 12:1193–1205
- Shin H, Santamarina JC (2013) Role of particle angularity on the mechanical behavior of granular mixtures. J Geotech Geoenviron Eng 139:353–355. https://doi.org/10.1061/(asce)gt.1943-5606. 0000768



- 43. Su D, Yan WM (2018) 3D characterization of general-shape sand particles using microfocus X-ray computed tomography and spherical harmonic functions, and particle regeneration using multivariate random vector. Powder Technol 323:8–23. https:// doi.org/10.1016/j.powtec.2017.09.030
- 44. Su D, Yan WM (2019) Prediction of 3D size and shape descriptors of irregular granular particles from projected 2D images. Acta Geotech. https://doi.org/10.1007/s11440-019-00845-3
- Sun Q, Zheng J (2019) Two-dimensional and three-dimensional inherent fabric in cross-anisotropic granular soils. Comput Geotech 116:103197. https://doi.org/10.1016/j.compgeo.2019.103197
- Sun Q, Zheng J (2019) Realistic soil particles generation based on limited morphological information by probability-based spherical harmonics. Comput Part Mech 6:1–21. https://doi.org/10.1007/ s40571-020-00325-6
- Sun Q, Zheng J, He H, Li Z (2019) Particulate material fabric characterization from volumetric images by computational geometry. Powder Technol 344:804–813. https://doi.org/10.1016/ j.powtec.2018.12.070
- Sun Q, Zheng J, Li C (2019) Improved watershed analysis for segmenting contacting particles of coarse granular soils in volumetric images. Powder Technol 356:295–303. https://doi.org/10. 1016/j.powtec.2019.08.028
- Sun Q, Zheng Y, Li B et al (2019) Three-dimensional particle size and shape characterisation using structural light. Géotechnique Lett 9:72–78
- Teh YW (2010) Encyclopedia of machine learning. Springer, Berlin
- Teh YW, Jordan MI, Beal MJ, Blei DM (2006) Hierarchical Dirichlet processes. J Am Stat Assoc 101:1566–1581. https://doi. org/10.1198/016214506000000302
- Vangla P, Roy N, Gali ML (2017) Image based shape characterization of granular materials and its effect on kinematics of particle motion. Granul Matter. https://doi.org/10.1007/s10035-017-0776-8
- Wadell H (1933) Sphericity and roundness of rock particles.
 J Geol 41:310–331. https://doi.org/10.1086/624040
- Wadell H (1932) Volume, shape, and roundness of rock particles.
 J Geol 40:443–451. https://doi.org/10.1086/623964
- Wadell H (1935) Volume, shape, and roundness of quartz particles. J Geol 43:250–280. https://doi.org/10.1086/624298
- Wei D, Wang J, Nie J, Zhou B (2018) Generation of realistic sand particles with fractal nature using an improved spherical harmonic analysis. Comput Geotech 104:1–12. https://doi.org/10. 1016/j.powtec.2018.02.006
- 57. Wei D, Wang J, Zhao B (2018) A simple method for particle shape generation with spherical harmonics. Powder Technol 330:284-291
- Zhao B, Wang J (2016) 3D quantitative shape analysis on form, roundness, and compactness with μCT. Powder Technol. https:// doi.org/10.1016/j.powtec.2015.12.029

- Zhao S, Zhao J (2019) A poly-superellipsoid-based approach on particle morphology for DEM modeling of granular media. Int J Numer Anal Methods Geomech 43:2147–2169
- Zheng J, Hryciw RD (2016) Index void ratios of sands from their intrinsic properties. J Geotech Geoenviron Eng 142:1–10. https:// doi.org/10.1061/(ASCE)GT.1943-5606.0001575
- Zheng J, Hryciw RD (2017) Particulate material fabric characterization by rotational haar wavelet transform. Comput Geotech 88:46–60. https://doi.org/10.1016/j.compgeo.2017.02.021
- Zheng J, Hryciw RD (2015) Traditional soil particle sphericity, roundness and surface roughness by computational geometry. Géotechnique. https://doi.org/10.1680/geot.14.P.192
- Zheng J, Hryciw RD (2017) An image based clump library for DEM simulations. Granul Matter 19:1–15. https://doi.org/10. 1007/s10035-017-0713-x
- Zheng J, Hryciw RD (2014) Soil particle size characterization by stereophotography. Geotechnical Special Publication, En, pp 64–73
- Zheng J, Hryciw RD (2017) Soil particle size and shape distributions by stereophotography and image analysis. Geotech Test J 40:317–328. https://doi.org/10.1520/GTJ20160165
- Zheng J, Hryciw RD (2016) A corner preserving algorithm for realistic DEM soil particle generation. Granul Matter 18:1–18. https://doi.org/10.1007/s10035-016-0679-0
- 67. Zheng J, Hryciw RD, Ohm H-S (2014) Three-dimensional translucent segregation Table (3D-TST) test for soil particle size and shape distribution. 3rd International symposium on geomechanics from micro to macro. Univ Cambridge, Cambridge, pp 1037–1042
- Zheng J, Hryciw RD, Ventola A (2017) Compressibility of sands of various geologic origins at pre-crushing stress levels. Geol Geotech Eng. https://doi.org/10.1007/s10706-017-0225-9
- Zheng J, Sun Q, Zheng H, Wei D, Li Z, Gao L (2020) Threedimensional particle shape characterizations from half particle geometries. Powder Technol 367:122–132. https://doi.org/10. 1016/j.powtec.2020.03.046
- Zhou B, Wang J (2016) Generation of a realistic 3D sand assembly using X-ray micro-computed tomography and spherical harmonic-based principal component analysis. Int J Numer Anal Methods Geomech 41:93–109. https://doi.org/10.1002/nag.2548
- Zhou B, Wang J (2015) Random generation of natural sand assembly using micro x-ray tomography and spherical harmonics. Géotechn Lett 5:6–11. https://doi.org/10.1680/geolett.14.00082
- Zhou B, Wang J, Zhao B (2015) Micromorphology characterization and reconstruction of sand particles using micro X-ray tomography and spherical harmonics. Eng Geol 184:126–137. https://doi.org/10.1016/j.enggeo.2014.11.009
- Zhou W, Yuan W, Ma G, Chang XL (2016) Combined finitediscrete element method modeling of rockslides. Eng Comput 33(5):1530–1559. https://doi.org/10.1108/EC-04-2015-0082

Publisher's Note Springer Nature remains neutral with regard to jurisdictional claims in published maps and institutional affiliations.



Terms and Conditions

Springer Nature journal content, brought to you courtesy of Springer Nature Customer Service Center GmbH ("Springer Nature").

Springer Nature supports a reasonable amount of sharing of research papers by authors, subscribers and authorised users ("Users"), for small-scale personal, non-commercial use provided that all copyright, trade and service marks and other proprietary notices are maintained. By accessing, sharing, receiving or otherwise using the Springer Nature journal content you agree to these terms of use ("Terms"). For these purposes, Springer Nature considers academic use (by researchers and students) to be non-commercial.

These Terms are supplementary and will apply in addition to any applicable website terms and conditions, a relevant site licence or a personal subscription. These Terms will prevail over any conflict or ambiguity with regards to the relevant terms, a site licence or a personal subscription (to the extent of the conflict or ambiguity only). For Creative Commons-licensed articles, the terms of the Creative Commons license used will apply.

We collect and use personal data to provide access to the Springer Nature journal content. We may also use these personal data internally within ResearchGate and Springer Nature and as agreed share it, in an anonymised way, for purposes of tracking, analysis and reporting. We will not otherwise disclose your personal data outside the ResearchGate or the Springer Nature group of companies unless we have your permission as detailed in the Privacy Policy.

While Users may use the Springer Nature journal content for small scale, personal non-commercial use, it is important to note that Users may not:

- 1. use such content for the purpose of providing other users with access on a regular or large scale basis or as a means to circumvent access control;
- 2. use such content where to do so would be considered a criminal or statutory offence in any jurisdiction, or gives rise to civil liability, or is otherwise unlawful:
- 3. falsely or misleadingly imply or suggest endorsement, approval, sponsorship, or association unless explicitly agreed to by Springer Nature in writing:
- 4. use bots or other automated methods to access the content or redirect messages
- 5. override any security feature or exclusionary protocol; or
- 6. share the content in order to create substitute for Springer Nature products or services or a systematic database of Springer Nature journal content

In line with the restriction against commercial use, Springer Nature does not permit the creation of a product or service that creates revenue, royalties, rent or income from our content or its inclusion as part of a paid for service or for other commercial gain. Springer Nature journal content cannot be used for inter-library loans and librarians may not upload Springer Nature journal content on a large scale into their, or any other, institutional repository.

These terms of use are reviewed regularly and may be amended at any time. Springer Nature is not obligated to publish any information or content on this website and may remove it or features or functionality at our sole discretion, at any time with or without notice. Springer Nature may revoke this licence to you at any time and remove access to any copies of the Springer Nature journal content which have been saved.

To the fullest extent permitted by law, Springer Nature makes no warranties, representations or guarantees to Users, either express or implied with respect to the Springer nature journal content and all parties disclaim and waive any implied warranties or warranties imposed by law, including merchantability or fitness for any particular purpose.

Please note that these rights do not automatically extend to content, data or other material published by Springer Nature that may be licensed from third parties.

If you would like to use or distribute our Springer Nature journal content to a wider audience or on a regular basis or in any other manner not expressly permitted by these Terms, please contact Springer Nature at

onlineservice@springernature.com